Sensors & Actuators: B. Chemical 344 (2021) 130301

Contents lists available at ScienceDirect

Sensors and Actuators: B. Chemical

journal homepage: www.elsevier.com/locate/snb

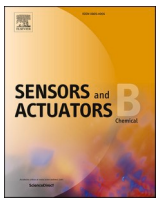

Handheld plasmonic biosensor for virus detection in field-settings

Arif E. Cetin [a,*], Zeynep A. Kocer [a,b], Seda Nur Topkaya [c], Ziya Ata Yazici [d]

[a] Izmir Biomedicine and Genome Center, Balcova, Izmir, 35340, Turkey
[b] Izmir International Biomedicine and Genome Institute, Dokuz Eylul University, Balcova, Izmir, 35340, Turkey
[c] Department of Analytical Chemistry, Faculty of Pharmacy, Izmir Katip Celebi University, Cigli, Izmir, 35620, Turkey
[d] Department of Biomedical Engineering, TOBB University of Economics and Technology, Cankaya, Ankara, 06560, Turkey

ARTICLE INFO

Keywords:
Plasmonics
Label-free biosensing
Point-of-care diagnostics
Nanotechnology
Lensfree-imaging

ABSTRACT

After World Health Organization (WHO) announced COVID-19 outbreak a pandemic, we all again realized the importance of developing rapid diagnostic kits. In this article, we introduced a lightweight and field-portable biosensor employing a plasmonic chip based on nanohole arrays integrated to a lensfree-imaging framework for label-free detection of viruses in field-settings. The platform utilizes a CMOS (complementary metal–oxide–semiconductor) camera with high quantum efficiency in the spectral window of interest to monitor diffraction field patterns of nanohole arrays under the uniform illumination of an LED (light-emitting diode) source which is spectrally tuned to the plasmonic mode supported by the nanohole arrays. As an example for the applicability of our biosensor for virus detection, we could successfully demonstrate the label-free detection of H1N1 viruses, e.g., swine flu, with medically relevant concentrations. We also developed a low-cost and easy-to-use sample preparation kit to prepare the surface of the plasmonic chip for analyte binding, e.g., virus-antibody binding. In order to reveal a complete biosensor technology, we also developed a user friendly Python™ – based graphical user interface (GUI) that allows direct access to biosensor hardware, taking and processing diffraction field images, and provides virus information to the end-user. Employing highly sensitive nanohole arrays and lensfree-imaging framework, our platform could yield an LOD as low as 10^3 $TCID_{50}$/mL. Providing accurate and rapid sensing information in a handheld platform, weighing only 70 g and 12 cm tall, without the need for bulky and expensive instrumentation, our biosensor could be a very strong candidate for diagnostic applications in resource-poor settings. As our detection scheme is based on the use of antibodies, it could quickly adapt to the detection of different viral diseases, e.g., COVID-19 or influenza, by simply coating the plasmonic chip surface with an antibody possessing affinity to the virus type of interest. Possessing this ability, our biosensor could be swiftly deployed to the field in need for rapid diagnosis, which may be an important asset to prevent the spread of diseases before turning into a pandemic by isolating patients from the population.

1. Introduction

Early detection and diagnosis of infectious diseases due to viruses is very critical for public and global health [1]. With the current SARS-CoV-2 (COVID-19) viral outbreak [2] (started around late 2019), many other viral pandemics, e.g., SARS [3] (2002–2004) and H1N1 or namely swine flu [4] (2009–2010) killed thousands of people in recent years. Despite the current diagnostic technologies, viral diseases still spread globally and turn into pandemics. During annual epidemics, rapid and accurate diagnostic technologies would be very useful in resource-poor settings. On the other hand, in the case of pandemics, these technologies could be swiftly modified and easily deployed to the required sites in an inexpensive way [5]. Current medical technologies for the diagnosis of viral diseases relying on polymerase chain reaction (PCR) [6], enzyme-linked immunosorbent assays (ELISA) [7] or cell cultures [8] require time-consuming and expensive procedures, bulky instrumentation necessitating sophisticated infrastructure, and trained laboratory professionals. Hence, their use in point-of-care diagnostics for viral diseases is not feasible. Especially for underdeveloped countries, the absence of medical infrastructure and healthcare professionals necessitates cost-effective and easy-to-use point-of-care diagnostic technologies. Such technologies could be an important asset for countries, lacking routine screening, to effectively deliver health services to individuals [9]. These technologies are also desired in developed

* Corresponding author.
E-mail address: arifengin.cetin@ibg.edu.tr (A.E. Cetin).

https://doi.org/10.1016/j.snb.2021.130301
Received 15 April 2021; Received in revised form 31 May 2021; Accepted 13 June 2021
Available online 16 June 2021

countries since the cost for healthcare is still a concern even if the resources are mostly available. Therefore, it is very critical to develop highly sensitive, easy-to-use and field-deployable point-of-care technologies with strong specificity for rapid and accurate diagnosis of viral diseases in resource-poor settings, which could prevent pandemics related to virus-borne diseases.

Label-free biosensors brought new modalities for the diagnosis of infectious diseases [10]. They are ideal for point-of-care diagnostics as (i) they could eliminate the need for optical or radioactive tags and enzymatic reactors, which suffer from cross-interference between labels and other molecular binding interactions, and (ii) overcome the problems due to insufficient number of labels as well as long and complex labeling steps. In literature, particularly three signal transduction mechanisms are proposed, e.g., optical [11,12], electrical [13,14] and mechanical [15] to generate label-free sensing information. Among those, optical biosensors are very popular thanks to their ability to allow remote signal transduction by forming light-matter interaction, which creates strong sensing signals that can be read out by an external detector. This is a strong advantage of optical biosensors over others, e.g., possessing a sensing mechanism that does not rely on a direct physical connection with the targeted analytes [16]. However, creating accurate and reliable sensing signals requires strong light-matter interaction that can be realized by systems precisely aligning light on the analytes of interest [17,18]. Therefore, most optical biosensors employ bulky and expensive tools, which are not ideal for field deployable point-of-care diagnostics.

Recently, subwavelength nanohole arrays have been proposed as a powerful candidate for point-of-care analyses due to their unique ability to confine normally illuminated light. Such geometry significantly simplifies optical alignment, which is very critical to realize field-deployable and robust biosensing platforms for field settings [19–22]. This modality of collinear configuration also allows signal evaluation with imaging devices within an array format, e.g., CCD (charge coupled device) or CMOS camera, instead of a photodetector or spectrometer, which enables multiplexed and high-throughput biosensing [23]. Allowing light transmission in a finite spectral window and filtering out the rest, nanohole arrays could yield sensing signal with high signal-to-noise ratio and minimum background noise [24]. Recently, plasmonic nanoholes have been also successfully used for the detection of pathogens, e.g., virus or bacteria [1,25–27]. Despite their performance on label-free detection of pathogens, biosensors utilizing nanohole arrays rely on benchtop instrumentation, which significantly limits their use in resource-poor settings. Therefore, there is a strong demand for low-cost and field deployable plasmonic platforms for label-free detection of pathogens [28]. Along this line, recently we have introduced a handheld plasmonic biosensor that combines lensfree-imaging with nanohole arrays for the detection of ultrathin protein layers towards label-free point-of-care applications [29]. By integrating a low-cost microfluidic chamber to this field deployable biosensor, we have successfully demonstrated the real-time analyses of protein binding kinetics in a multiplexed manner [30]. To our knowledge, nanohole array-based biosensors integrated with lensfree-imaging technology have not been offered for the detection of viruses in resource-poor settings yet.

In this article, we introduced a handheld biosensor that combines plasmonic label-free sensing technology with lensfree computational imaging for point-of-care diagnosis of viral diseases. As an example, we demonstrated the label-free detection of H1N1 influenza virus that caused swine flu in 2009, and established in human as a seasonal influenza strain since then. We also developed a sample preparation kit to ensure a plasmonic sensor chip with strong affinity to H1N1 influenza viruses via antibody-based surface modification. The sample preparation kit also ensures the minimum consumption of consumables providing the largest sensing signal with the handheld biosensor. In addition to our effort on hardware advancement, we also developed a Python™ – based software that allows the acquisition and evaluation of diffraction field images to provide virus information to the operator. The platform employs a very simple optics using affordable components, which are aligned within a dark environment without the need for optical or mechanical instrumentation. Thanks to its compact and lightweight design, e.g., only 12 cm tall and weighing 70 g, as well as strong sensing capability with minimum detectable H1N1 virus concentration of 10^3 $TCID_{50}$/mL, our handheld biosensor is a strong candidate for point-of-care diagnostic applications for viral diseases.

2. Results and discussion

2.1. Components of the handheld plasmonic biosensor

Fig. 1A shows the photograph of the handheld plasmonic biosensor. As shown in Fig. 1B, the biosensor is constituted by three components: (i) A plasmonic chip composed of subwavelength nanohole arrays fabricated through a thin gold film. These apertures support strong electromagnetic fields localized around the rims of the nanoholes, and extend extensively into the medium. Hence, the transmission resonance supported by plasmonic nanoholes, related to their extraordinary light transmission (EOT) property, is very sensitive to change within the refractive index in the vicinity of the sensor surface. Then, the viruses are detected via the spectral variations within the EOT signal due to the refractive index changes that are triggered by the presence of viruses captured on the plasmonic surface. (ii) An LED light source that spectrally overlaps with the plasmonic mode of the chip. (iii) A CMOS camera that records the diffraction field intensities of the nanohole arrays. Fig. 1C shows the real picture of the sample preparation kit. Sample preparation kit divides the plasmonic chip into two compartments, sensor and control, where the sensor region is coated with antibodies specific to H1N1 viruses, and the control region is used to determine any optical or mechanical fluctuations (Fig. 1D). Spectral variations within the nanohole response result in a better spectral match between EOT signal and LED response. Thus, the captured viruses on the sensor region increases the diffraction field intensity compared to control region (schematically illustrated in Fig. 1B).

2.2. Fabrication of the plasmonic chips

Plasmonic nanohole arrays were realized through a high-throughput and wafer-scale fabrication method based on deep-UV lithography [24,31,32]. In this article, our goal is to develop an affordable label-free biosensor, i.e., we employed a fabrication method which enables the realization of nanoholes in a low-cost manner compared to the classical manufacturing techniques. As opposed to E-beam lithography, where nano-features are created sequentially, our technique enables parallel fabrication of nanohole arrays in wafer-scale, which dramatically lowers the cost and duration of the nano-fabrication. Fig. 2A shows the schematic illustration of the fabrication steps. We carried out the fabrication protocol on a 500-μm thick 4-inch fused silica (glass) wafer, coated with 100 nm LPCVD (low pressure chemical vapor deposition) silicon nitride (SiN) film. This SiN film is optically transparent, and functions as a high refractive index interlayer that yields an isolated transmission resonance by eliminating unwanted plasmonic modes excited along the interface between Au and fused silica [33]. (i) We first deposited 5 nm Cr, functioning as an adhesion layer, and 120 nm Au. This optically thick Au layer ensures a transmission spectrum solely due to the plasmonic effects excited by the nanohole arrays via blocking light transmission in nanohole-free locations. (ii) We then performed deep-UV lithography on a positive resist coated on the wafer surface, where the mask allows the formation of nanohole features throughout the resist. (iii) After the development, we etched the metal film via dry etching using SF_6 and Ar (reactive ion etching), while the photoresist was used as a mask, revealing the nanohole patterns through the Au film. (iv) Finally, we removed the remaining resist on the Au surface with O_2 plasma cleaning. With this fabrication technique, nanoholes could be realized in

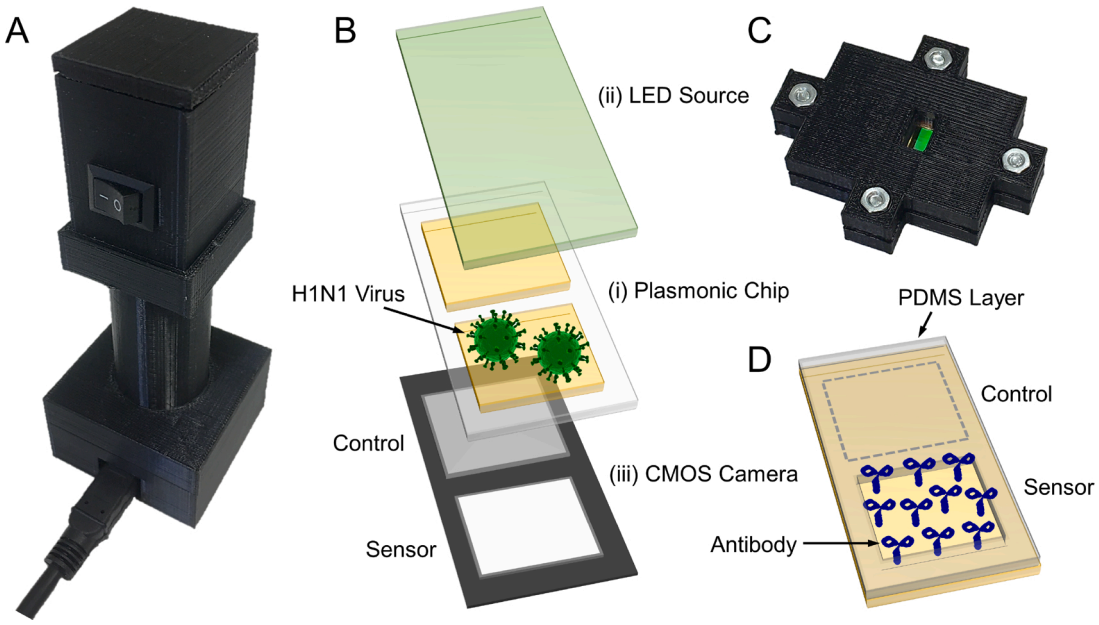

Fig. 1. Photograph and schematic illustration of (A, B) the handheld plasmonic biosensor and (C, D) the sample preparation kit. Sample preparation kit divides the plasmonic chip into sensor and control regions, which have different diffraction field intensities under the same LED illumination captured by the CMOS camera.

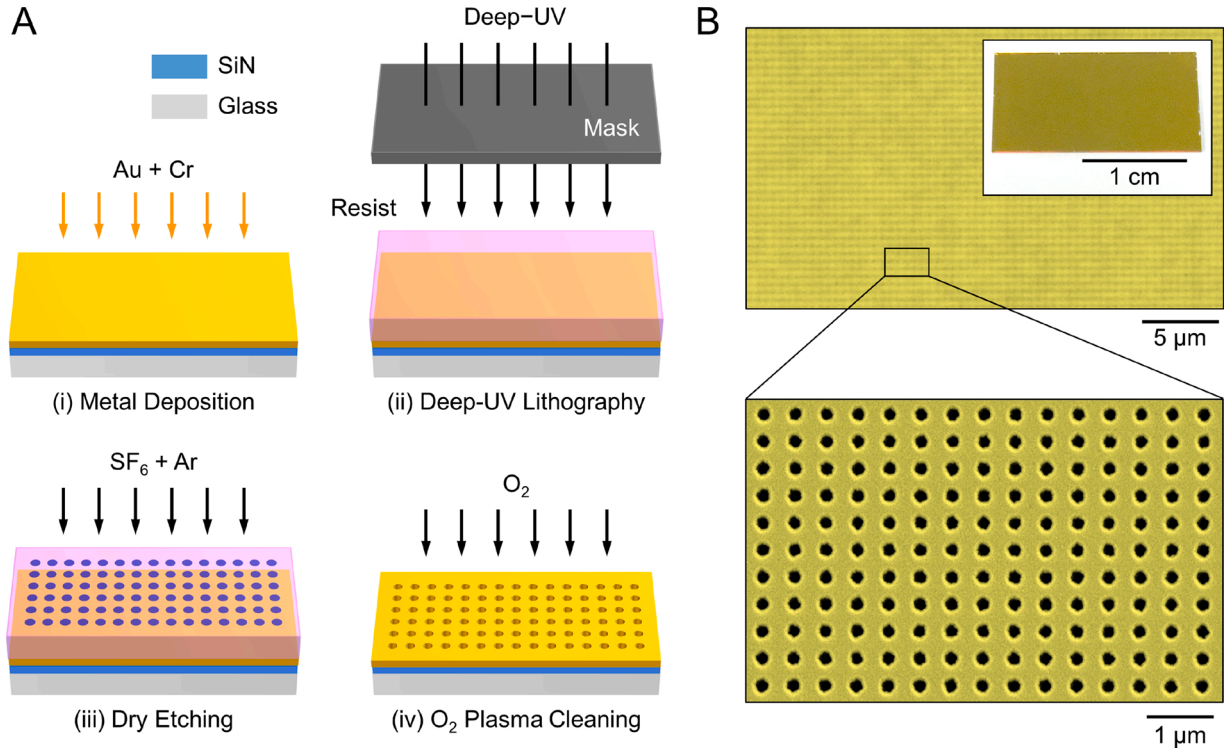

Fig. 2. (A) Schematic illustration of the wafer-scale and low-cost fabrication method based on deep-UV lithography for high-resolution plasmonic nanohole arrays. The corresponding device parameters: Hole diameter = 190 nm, Array periodicity =450 nm, Au thickness = 120 nm, Cr thickness =5 nm, SiN thickness: 100 nm. (B) Top: Optical microscope image of the nanohole arrays. Top-inset: Photograph of a 2 cm × 1 cm plasmonic chip. Bottom: SEM image of the nanohole arrays.

wafer-scale, i.e., we diced the wafer to realize plasmonic chips with the desired dimensions. Fig. 2B-top shows the photograph of the plasmonic chip with 2 cm × 1 cm dimension. The optical microscope image (Fig. 2B-top) demonstrates that the nanohole arrays are uniform over a very large area. Scanning electron microscope (SEM) image (Fig. 2B-bottom) shows the nanoholes with 190 nm diameter and 450 nm array periodicity, demonstrating the quality and resolution of our fabrication method. This hole size allows sufficient light transmission for creating reliable sensing signal without distorting the transmission resonance supported by the nanohole arrays.

2.3. Sample preparation kit

Since the label-free nature of our biosensor relies on virus specific antibodies, it is vital to provide accurate sensing data with low amount of capturing ligands, which is the key asset to develop an affordable

point-of-care diagnostic platform.

In our biosensor platform, spectral readout is implemented by monitoring the diffraction field intensity of the plasmonic mode supported by the nanohole arrays. Therefore, for data generation, only the location on the plasmonic chip that matches with the CMOS active area is critical. For this particular reason, we designed the sample preparation kit in such a way that the solution containing the targeted analytes is pipetted and incubated on the plasmonic chip surface from an opening (functions as an incubation chamber) that allows binding only on the required chip surface. Fig. 3A shows the photograph of the sample preparation kit which is composed of (i) two polydimethylsiloxane (PDMS) sealing layers, and (ii) two polylactic acid (PLA) locking caps. Fig. 3B shows the schematic illustration of the manufacturing process for these constituting parts. Shape of the PDMS layers was determined with two PLA molds manufactured with 3D-printing (See Supporting Fig. SI1 for the photograph of the PLA molds and PDMS layers). As shown in the figure, the top PDMS layer has a rectangular hole that ensures a leak-free incubation along the desired location on the plasmonic chip surface. The bottom PDMS layer has a rectangular space, where the plasmonic chip is positioned. Plasmonic chip is then sandwiched between two PDMS layers (schematically shown in Fig. 3C), and this sandwich is inserted between two PLA caps functioning as a locking mechanism using four screws on sides (See Supporting Fig. SI2 for the photograph of the locking mechanism). Here, the deformability of the PDMS layers allows screw tightening to such an extent that is sufficient for sealing without damaging the 0.5-mm-thick plasmonic chip. Fig. 3C schematically shows the sample preparation kit during the incubation phase, where the analytes cover only the portion of chip surface that matches with the half of the CMOS active area. For the label-free detection of viruses, this area functions as sensor (blue), while the rest is used for control (yellow).

2.4. Optical instrumentation of the portable biosensor

The basic working principle of the portable biosensor is to capture diffraction field images of the plasmonic chip by the CMOS camera and to determine spectral variations within the nanohole EOT response by tracking the intensity variations before and after analyte binding. Limit-of-detection of the system, (in other words, minimum detectable virus concentration) corresponds to the lowest virus concentration that create a change in the diffraction field intensity which can be detected by the CMOS camera. Therefore, LED light source and CMOS camera should be chosen to provide an ability to create and monitor diffraction field intensity changes even in the presence of very low virus concentrations. Fig. 4A shows these components, where bottom PLA part contains the USB-powered CMOS camera, and top PLA part contains the battery-powered LED light source. Here, an inter-PLA tube (not shown in the figure) was used to create a uniform LED illumination along the CMOS active area. The top PLA part has a circuit composed of a battery, a switch button to turn on/off the light source and a resistor lowering the LED brightness to prevent the camera saturation. In the bottom PLA part, plasmonic chip is positioned inside a square groove having the same dimension with the chip to accurately match the sensor and control regions with the active area of the CMOS camera. There are two oval shaped grooves on the sides in this square to position/take the chip from the biosensor. Here, there are two important criteria to choose the proper components: (i) LED source should have a narrow bandwidth, and spectrally position very close to the nanohole EOT response, and (ii) CMOS camera should have a high quantum efficiency within the spectral range that covers both EOT signal and LED response [29,30,34]. Fig. 4B shows the EOT response of the plasmonic chip positioned at ~550 nm (grey), the power output of the LED source positioned at ~573 nm (green), and the quantum efficiency of the CMOS camera (red). Here, the narrow bandwidth of the LED source, e.g., 10 nm, and the near-uniform quantum efficiency of the CMOS camera within the spectrum of interest are very critical to reliably create the diffraction field intensity variations in the presence of very low analyte concentrations.

2.5. Label-free detection of H1N1 influenza virus

The biosensor platform enables label-free detection via attaching the targeted analytes on the surface of the plasmonic substrate with capturing ligands, which triggers a spectral shift within the EOT response of the nanohole arrays. Here, we first employed a cleaning procedure to ensure a plasmonic chip chemically favorable for label-free virus detection as explained in the Experimental Section. In order to capture H1N1 viruses on the chip surface, we used a surface modification technique, which does not require complex and long preparation time. This technique also allows chip-recycling via removing the organic contaminants with a simple cleaning procedure since it does not rely on strong and irreversible molecular bonds between analytes and the Au surface (See Experimental Section for the details of the analyte

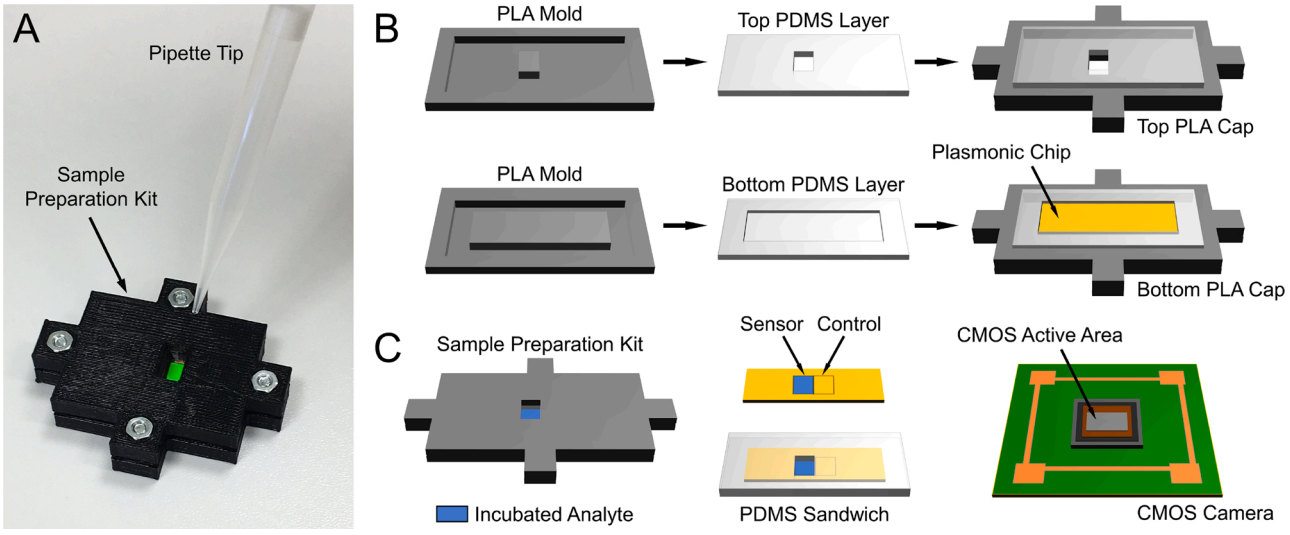

Fig. 3. (A) Photograph of the sample preparation kit, where the analyte solution is injected with a pipette to the surface of the plasmonic chip through the rectangular hole in the top part of the kit. (B) Schematic illustration of the PLA molds used to manufacture PDMS layers that ensures a leak-free analyte incubation on the plasmonic chip surface. (C) Plasmonic chip is sandwiched between PDMS layers which is then inserted between two PLA caps. Sample preparation kit creates an analyte-coated spot (blue) which is half of the CMOS active area in size, and forms two locations on the camera screen, e.g., sensor and control.

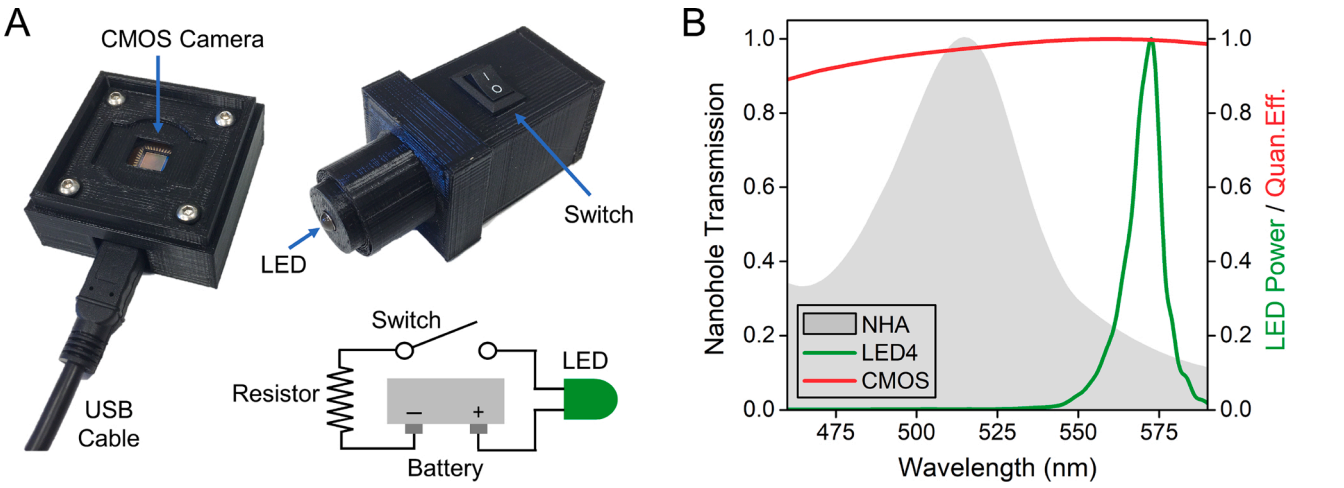

Fig. 4. (A) Photograph of the two main optical components of the portable biosensor: USB-powered monochromatic CMOS camera (Thorlabs), and battery-powered LED light source (Digi-Key Electronics). Figure inset: Schematic illustration of the electrical circuit for controlling the light source. (B) EOT response of the nanohole array (grey), power output of the LED light source (green), and quantum efficiency of the CMOS camera (red).

immobilization technique). Surface modification was carried out with the sample preparation kit, where the corresponding solutions were pipetted to/back and incubated in each step. Between each step, sample preparation kit was opened using the screws on sides, and the plasmonic chip was rinsed with PBS (phosphate-buffered saline) and DI-water. With this step, the unbound proteins and the proteins on the surface due to non-specific adsorption were removed from the plasmonic chip surface. Fig. 5A shows the schematic illustration of an H1N1 virus captured on the sensing surface. After cleaning, Au surface was coated with protein A/G. We then introduced protein IgG on the A/G coated Au surface. The virus antibody has two subdomains, e.g., Fab and Fc. Due to the high affinity of protein A/G to the Fc region of the virus antibody, protein IgG positions on the protein A/G forming a "Y" shape, i.e., its glycoprotein binding sites are freely exposed. Then, the virus attaches on the virus antibody through its hemagglutinin (HA) glycoproteins. Fig. 5B shows the SEM image of the H1N1 viruses on the nanohole surface.

Fig. 5C shows the EOT response of the nanohole arrays before and after the attachment of analytes on the sensing surface (See Experimental Section for the details of the spectral analyses). The increase in the total biomass due to the analyte accumulation increases the effective refractive index in the vicinity of the sensing surface, e.g., shifting the EOT response to longer wavelengths. For example, EOT response initially located at ~514 nm (black)shifted to ~519 nm (red) and ~532 nm (blue) after the addition of 200 μg/mL protein A/G and 100 μg/mL protein IgG, respectively. Here, we used very high protein concentrations ensuring the saturation of the sensing surface with virus antibody for accurately capturing viruses on the surface, which creates sufficient sensing signals to be able to read with the CMOS camera even in the presence of very low virus concentrations. In this section, in order to demonstrate the working principle of our biosensor, we used a high virus titer, e.g., 10^7 $TCID_{50}$/mL, where the presence of the H1N1 viruses shifted the EOT resonance to ~551 nm (green).

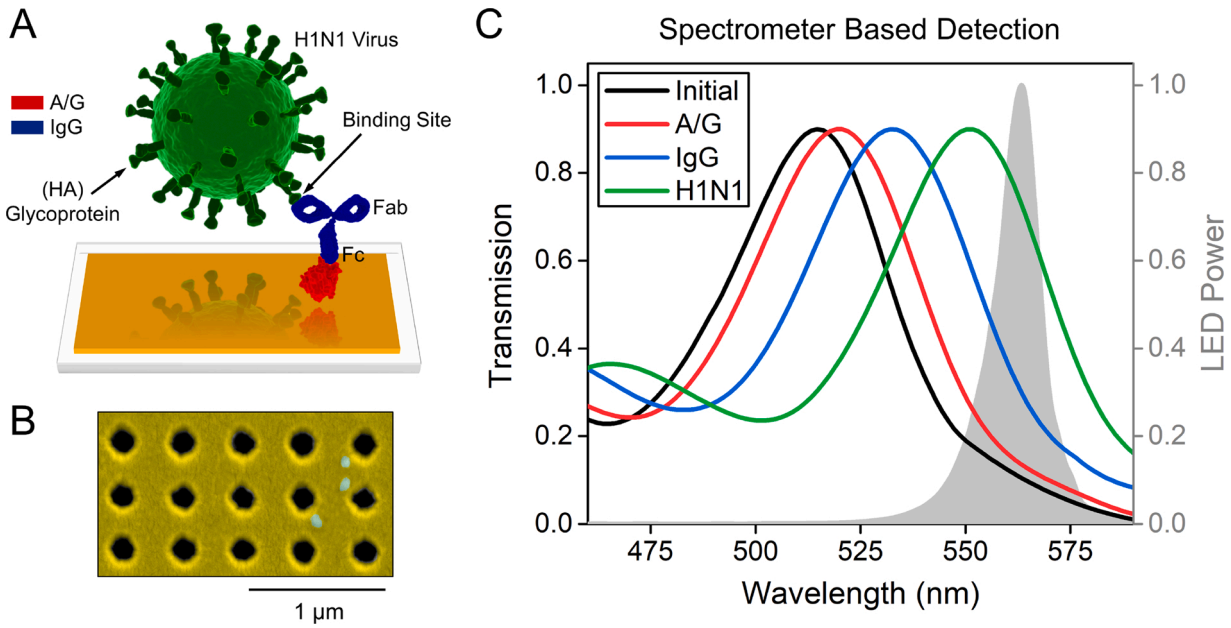

Fig. 5. (A) Schematic illustration of the virus (green) attachment on the Au surface using protein A/G (red) and virus antibody (blue). (B) SEM image of the H1N1 viruses on the surface of the Au nanoholes. (C) EOT response of the nanohole arrays before (black) and after the attachment of protein A/G (red), protein IgG (blue) and H1N1 virus (green). Gray denotes the output power spectrum of the LED light source used in the portable biosensor platform.

2.6. Using CMOS diffraction images for label-free detection

In our portable biosensor, the LED spectrum (gray curve in Fig. 5C) was positioned at longer wavelengths compared to the EOT response of the nanohole arrays (black curve in Fig. 5C), e.g., as the EOT resonance shifts toward longer wavelengths with analyte binding, it better overlaps with the LED power spectrum. Better spectral overlap enables higher number of photons reaching the camera, which causes an increase in the diffraction field intensity in the sensor location (See Supporting Fig. SI3 for the schematic illustration of this phenomenon). For instance, Fig. 6A shows the diffraction field intensity images captured by the CMOS camera, demonstrating the distinct difference between control and sensor regions coated with protein IgG. As shown in Fig. 6B, LED source illuminating the plasmonic chip creates a uniform diffraction field disturbed across the chip surface, which is very advantageous for reliable image processing. Fig. 6C shows the diffraction field intensities calculated for control (orange line) and sensor (black line) regions before and after analyte binding on the surface of the plasmonic chip. These values were determined by taking the average of the diffraction field intensities in a 0.5 mm × 0.5 mm area denoted with white squares in Fig. 6A. The intensity changes in the diffraction field images with analyte binding in the sensor region could be easily differentiated with naked eye (Fig. 6C-inset). On the other hand, for the control region, diffraction field intensity does not show any variation due to the absence of spectral variations within the nanohole EOT response, demonstrating the reliability of our label-free detection technique.

2.7. Detection limit of the portable platform

False positive is the most important challenge that could weaken the reliability of biosensors. Most plasmonic biosensors provide the label-free sensing information based on sensing-by-binding type surface modification techniques, e.g., the analyte that needs to be detected should be attached on the sensing surface. Therefore, it is very critical to ensure specificity, which is the most important asset for eliminating false positive in the presence of other potential pathogens that could bind on the surface. In our biosensor, specificity is provided by the IgG antibody (anti-swine H1N1 hemagglutinin, Merck KGaA), which has affinity only to H1N1 viruses. In order to demonstrate the specificity of our biosensor, we compared the spectral variations within the nanohole EOT response due to the presence of H1N1 viruses, where the sensing surface is covered with control (anti-Vesicular stomatitis virus antibody, Merck KGaA) and H1N1 antibodies. Fig. 7A (black curve) and 7B (blue curve) show the EOT response of the nanohole arrays coated with control and H1N1 antibodies. As the molecular weights of these antibodies are very similar, there is only 1 nm difference between spectral positions of the EOT response for control and H1N1 antibodies. After the virus incubation, EOT response shifts to longer wavelengths (Fig. 7B, green curve) due to H1N1 viruses binding on H1N1 antibody coated Au surface. On the other hand, no spectral variation was observed within the EOT response after the virus incubation for the nanohole surface coated with control antibody (Fig. 7A, dashed red curve) since viruses were not captured by the control antibodies, and removed from surface during the rinsing process. This result clearly demonstrates the specificity of our sensing technique to H1N1 influenza viruses.

In addition to specificity, it is also very critical to provide accurate sensing data in the presence of very low analyte concentrations. To generate a sensing signal in classical plasmonic systems, spectral position of transmission or reflection maxima is monitored, which corresponds to the plasmonic mode excited by the nano-features employed in the system [1]. The major disadvantage of this method is its low limit-of-detection as it depends only on a single spectral data. For instance, in the presence of low number of analytes, the change within the effective refractive index of the medium in the vicinity of the plasmonic substrate could be very weak, i.e., it may not create sufficient spectral variations within the plasmonic response [24,31,34,35]. In order to address this problem, instead of monitoring spectral variations at a single wavelength, we cumulatively monitored spectral variations within multiple wavelengths around the EOT response. Hence, more sensitive sensing data could be created compared to the one relying only on a single spectral position. In order to consider multiple spectral variations, we calculated the integral of EOT response within a 35-nm-wide spectral window highlighted with a gray area in Fig. 7B. Here, specifying the spectral position of the integral window is very critical to reliably provide sensing signals. Considering the Lorentzian shape of the EOT response and the spectral position of the EOT response determined for the largest virus titer, e.g., 10^7 $TCID_{50}$/mL, positioning at ~551 nm, we positioned the spectral window at 553 nm. Consequently, the maximum of the EOT response for each virus titer positions at shorter wavelength compared to the integral window. Hence, for the calculation of the spectral integral, only the transmission values on the right side of the EOT resonance were used, which prevents any

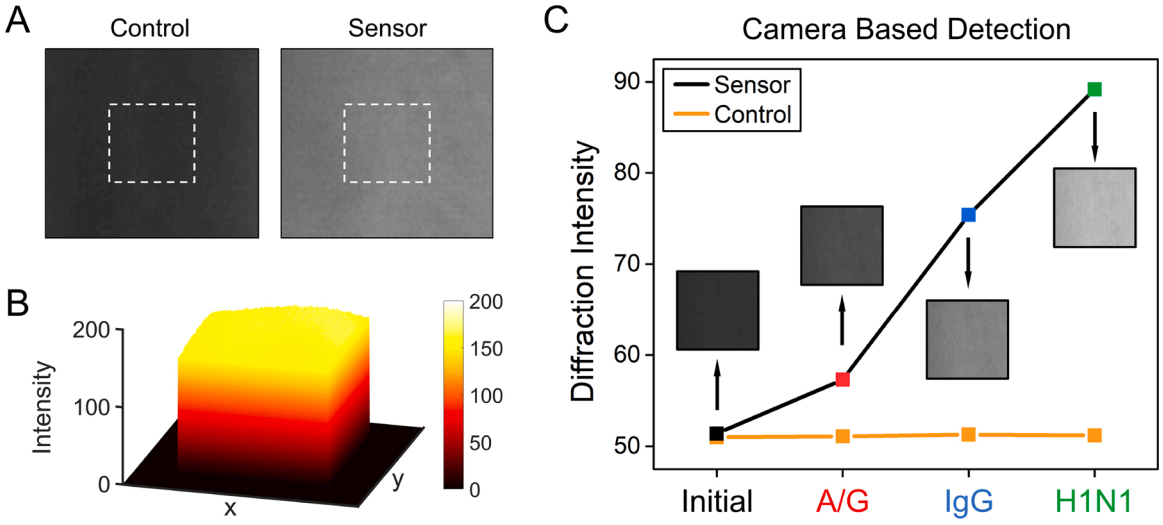

Fig. 6. (A) The CMOS camera image showing control and sensor regions on the plasmonic chip. (B) 3D-representation of the diffraction field distributed across the sensor region. (C) Average diffraction field intensities calculated for control (orange) and sensor (black) regions upon the binding of protein A/G, protein IgG and H1N1 virus. Calculations were performed in the regions denoted with white squares in Fig. 6A. Figure inset shows the real CMOS images of the sensor region for each binding step.

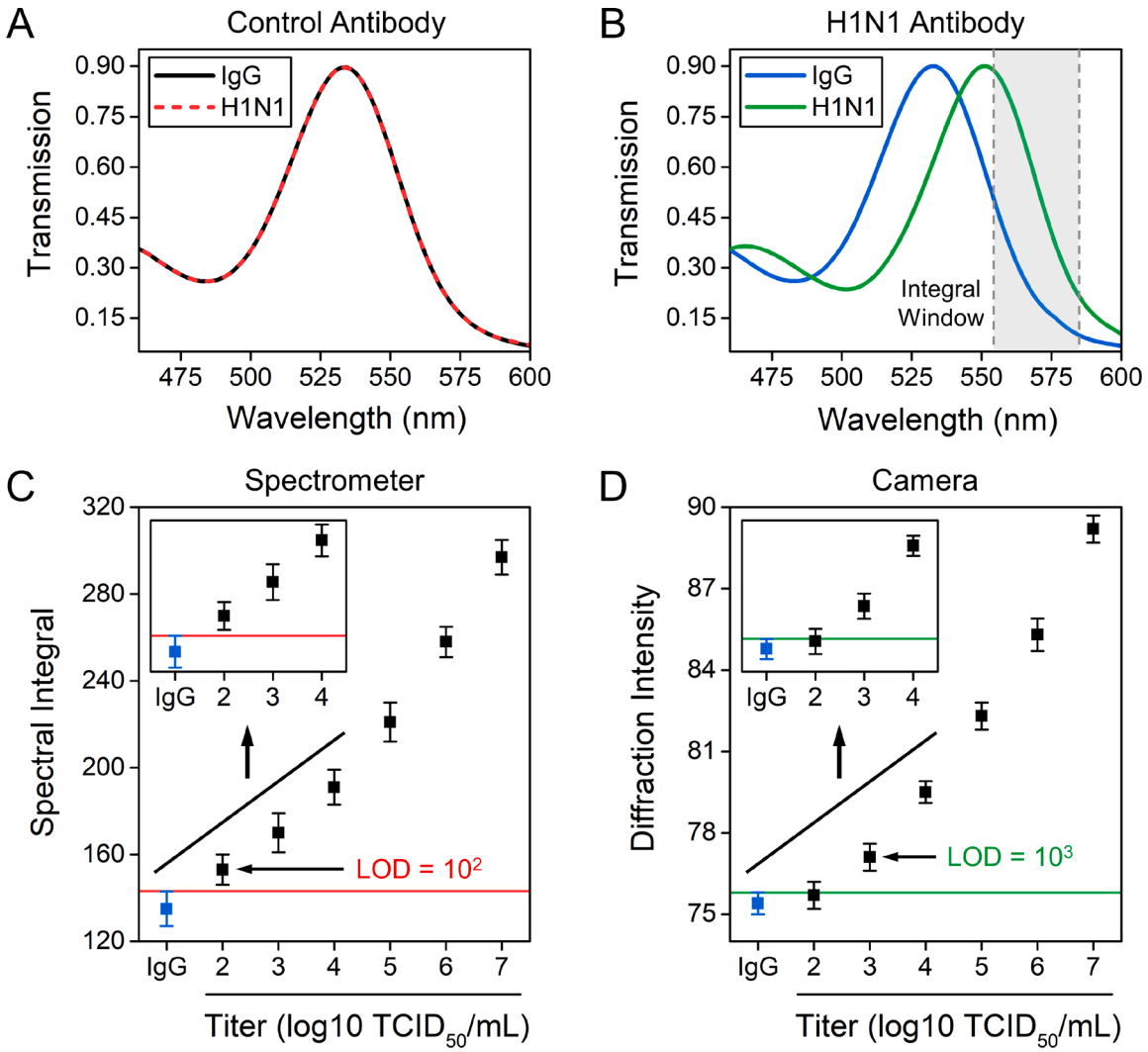

Fig. 7. (A) EOT response after the addition of control antibody (black) and H1N1 virus (red). H1N1 virus does not lead any spectral variation within the EOT response of the control antibody-coated nanohole arrays. (B) EOT response after the addition of H1N1 antibody (blue) and H1N1 virus (green). H1N1 virus shifts the EOT response of the H1N1 antibody-coated nanohole arrays to longer wavelengths. (C) Spectral integral values determined by the spectrometer-based read-out scheme, and (D) diffraction field intensity values determined by the camera-based read-out scheme employed in the portable biosensor for different virus titers. The figure shows the mean values with error bars, twice the standard deviation from three independent experiments. Figure insets show the zoom to the lowest virus titers for better resolution for LOD determination. LOD's for both techniques were highlighted with red (spectrometer) and green (camera) lines.

miscalculation due to the Lorentzian shape of the EOT resonance.

Fig. 7C shows the spectral integral values calculated for different virus titers. Here, as the virus titer increases, the number of H1N1 virus attaching on the gold sensing surface increases. The increase in the accumulated biomass on the sensor surface increases the effective refractive index, which shifts the EOT resonance to longer wavelengths. Thus, the EOT response and the integral window better spectrally overlap, i.e., larger transmission values fall into the integral window, and the spectral integral value increases accordingly. Here, we used the virus titers, e.g., 10^2, 10^3, 10^4, 10^5, 10^6 and 10^7 $TCID_{50}$/mL. Solutions with different virus titers were incubated on separated locations on the same plasmonic chip. Using the same chip for all virus titers eliminates any contribution from the plasmonic chip on determining system LOD. We pipetted samples containing 10 μL virus solution prepared in sterile PBS that covers an area of 350 μm diameter on the plasmonic chip surface. Such area on the chip surface contains a number of nanoholes providing sufficient signals for both spectrometer- and camera-based spectral read-out [23]. Figure shows the mean spectral integral values (black squares) of three independent experiments with error bars twice the standard deviation (SD). For each concentration, we calculated the relative standard deviation (RSD = 100 × SD / mean), where we showed excellent repeatability, e.g., 5.93 %, 4.58 %, 5.29 %, 4.19 %, 4.07 %, 2.71 %, and 2.69 % for IgG, 10^2, 10^3, 10^4, 10^5, 10^6 and 10^7 $TCID_{50}$/mL virus titer, respectively. The spectral integral value for each virus titer could be distinguished from the initial integral value (blue square corresponds to the EOT response of the IgG coated nanohole arrays). Thus, the LOD for the classical spectrometer-based platform was determined as 10^2 $TCID_{50}$/mL, highlighted with a red line in Fig. 7C.

Finally, we determined the LOD of the portable biosensor employing camera-based spectral read-out. Fig. 7D shows the diffraction field intensity values determined for each virus titer, e.g., the mean values (black squares) with errors bars of twice the standard deviation determined from 3 independent experiments. In order to ensure a fair comparison between two techniques, we used the same plasmonic chips for spectrometer- and camera-based experiments. For each concentration, we calculated RSD as 0.53 %, 0.66 %, 0.65 %, 0.50 %, 0.60 %, 0.70 %, and 0.56 % for IgG, 10^2, 10^3, 10^4, 10^5, 10^6 and 10^7 $TCID_{50}$/mL virus titer, respectively, which demonstrates their excellent repeatability. Here, the diffraction field intensity created by each titer could be differentiated from the initial value, except the one determined for 10^2

$TCID_{50}$/mL. Hence, for the portable biosensor, LOD was found as 10^3 $TCID_{50}$/mL, highlighted with a green line in Fig. 7D. Despite holding a great promise as a field-deployable and cost-effective device, our portable biosensor provides higher LOD compared to its classical plasmonic counterpart based on an expensive, bulky and high-resolution spectrometer setting. This is due to the spectral resolution of our platform, which could not be sufficient to differentiate analyte concentrations detected by the spectrometer-based setup. As shown in the Experimental Section, we utilized a spectrometer with a spectral resolution, as low as, 0.09 nm, which is ultra-sensitive to minute spectral variations. Therefore, sensitivity of our handheld platform should be improved to detect virus titers in this level without sacrificing from portability, lightweight, compactness and low-cost which are very critical for point-of-care diagnostics. We discussed possible improvements along this line in the last section.

2.8. Graphical user interface of the portable platform

In order to evaluate the plasmonic chip through the CMOS camera, and provide the sensing information to the end-user via image processing, we developed a Python™ – based GUI. As shown in Fig. 8, the program can directly access the camera settings, and allows the operator to choose the best parameters for the test. After placing the plasmonic chip in front of the CMOS camera, and connecting to the camera through GUI, the operator could see the diffraction image of the control and sensor regions which are digitally separated with a white column. The operator then takes an image and clicks on the run test button. Then, GUI determines the average diffraction intensity values in the region denoted with white squares. As determined in the previous section, LOD of the portable system is 10^3 $TCID_{50}$/mL, where we can reliably determine the presence of H1N1 viruses. Here, GUI uses the ratio between the diffraction field intensities of sensor and control regions for 10^3 $TCID_{50}$/mL. Running the test, the program calculates the ratio between sensor and control, and if the calculated value is larger than the one determined for the LOD condition, GUI shows a warning sign for virus detection to the operator. Such approach eliminates any external effects with the use of diffraction field intensity images of the control region, which yields a sensing data solely related to the targeted analytes. This user-friendly program could be very advantageous for field operations as it does not require the need for well-trained professionals.

3. Conclusion and future work

In this article, we introduced a handheld biosensor that employs a plasmonic chip based on subwavelength nanohole arrays integrated to a lensfree-imaging framework. The biosensor uses a CMOS camera to record diffraction field intensities of nanohole arrays under an LED light source tuned to the plasmonic mode of interest. The platform could successfully detect H1N1 viruses with medically relevant concentrations. We also developed a sample preparation kit to minimize consumable consumption without sacrificing from the sensitivity. In addition to the hardware development, we also developed a GUI that controls the CMOS camera, and provides the sensing information based on diffraction field images.

Currently, human H1N1 influenza is diagnosed by real-time PCR detection and characterization panel, which could provide very sensitive and specific test results within approximately 4 h. On the other hand, antigen tests detect proteins on the surface of the viruses and could provide the virus information, i.e., the tested individual is infectious. Antibody tests detect antibodies against the viruses and determine the presence of viruses while not detecting an active infection. Unlike PCR, these two affordable approaches, mainly depended on a lateral flow scheme, could provide rapid test results without the need for bulky and expensive instrumentation as well as healthcare experts. However, antigen tests could provide false negative results in the presence of low virus level, while antibody tests possess low accuracy. Here, providing accurate sensing data in a field-deployable and lightweight platform, our biosensor could be a strong candidate for the diagnosis of pathogen-based diseases in a cost-effective manner compared to its classical diagnostic counterparts.

In this section, we also discussed possible improvements that will not only address the problems related to the sensing capability of the biosensor, but also the requirements for its commercialization. Optical sensitivity of the platform could be further improved by exciting plasmonic modes with much shaper EOT signals and larger nearfield intensities, e.g., Fano-resonant apertures, [36–38] or nano-gap features [39,40]. Employing excitation sources with narrower bandwidths, e.g., laser diodes, phosphor-coated or resonant-cavity enhanced LEDs could also dramatically improve optical sensitivity. Sensing information could be more accurate by creating more sensitive diffraction images with the use of multiple light sources. For example, employing multiple LED sources could create simultaneous diffraction images on the CMOS camera like in pinhole camera settings to monitor spectral variations at different spectral locations [30]. Sequentially taking CMOS images for

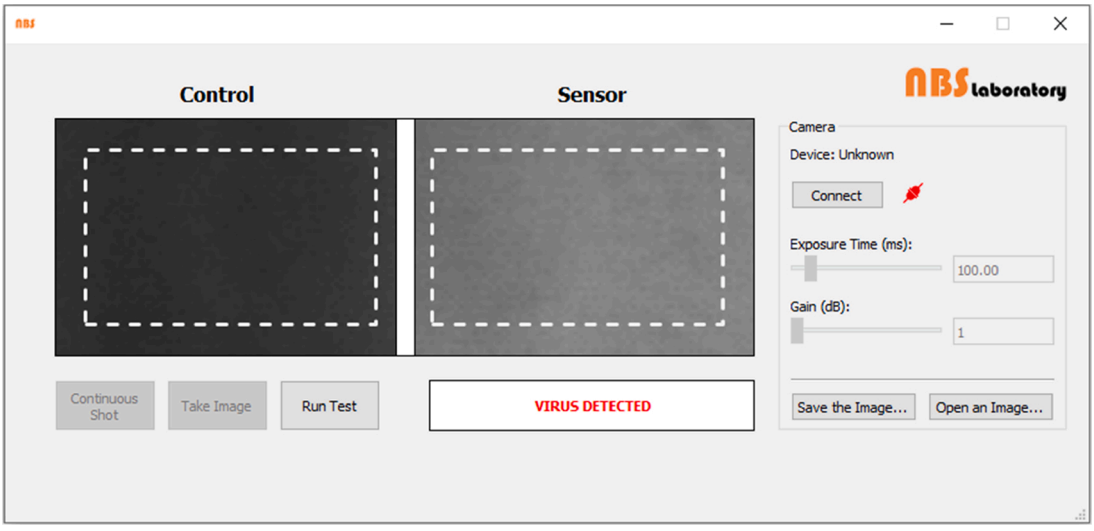

Fig. 8. GUI of the handheld biosensor providing virus information by taking and processing the diffraction field image of the plasmonic chip. In the figure, GUI detects the presence of H1N1 viruses in sample.

different light sources could be also digitally merged to produce higher contrast between sensor and control regions [23]. Accuracy and sensitivity of the CMOS camera could be improved by equipping it with a cooling circuit or an apparatus.

In our handheld biosensor, we utilized a simple physisorption based surface modification method to reuse the plasmonic chips after a cleaning protocol, where the weak bonding of analytes on the sensing surface could be easily removed. However, towards commercialization, chip recycling could negatively affect test reliability, and the plasmonic chip should be provided as one-time-use in the presence of a deadly virus for biosafety concerns. Moreover, the plasmonic chip should be ready-to-use, where the surface is already coated with virus specific antibodies as in the commercial SPR platforms. Therefore, the antibodies should be strongly attached on the metal, stay stable for long period of time (long shelf life), and provide a uniform analyte coating on the sensor region. This could be realized by immobilizing antibodies on the surface via PEGylated self-assembled monolayer (SAM) that could provide antifouling and stable coating, [41] where biotin related antibodies are attached on SAM coated sensing surface through streptavidin [25]. For the plasmonic chips in ready-to-use format, further characterization tests should be performed to determine the optimum wait duration providing a reliable sensing signal. For this proof-of-principle work, we incubated the viruses for 1 h on sensor surface to ensure the maximum sensing signal. This duration could be shortened to sub-10 min since vast amount of analyte binding occurs within the first couple of minutes as it could seen with the real-time analyte binding experiments [41].

Sensitivity of the platform could be further improved with nanoparticle based assays functionalized on the sensing surface by increasing the analyte binding sites [19]. The plasmonic chip could be manufactured in a microarray format (to realize multiple sensor locations) via, e.g., depositing a metal layer in a well-defined pattern on the plasmonic chip by photolithography [23]. Hence, same pathogen test could be simultaneously performed in multiple locations on the same chip, which could bring high-throughput functionality, thus test reliability. Using the same micro-array format, multiple antibodies could be used to detect different pathogens at the same time, which is vital for the diagnostic of diseases related to multiple pathogens [41].

4. Experimental section

4.1. Chip cleaning

Fabrication of the plasmonic chips was performed on wafer-scale, and the plasmonic chips with desired dimensions were prepared with a wafer cutter. Here in order to protect the nanohole features, the wafer surface was covered with a polymer. This polymer layer was removed with piranha cleaning, composed of 3:1 sulfuric acid: hydrogen peroxide. Piranha solution could be also used to remove residues at the end of each test for chip-recycling. In addition to removing organic and inorganic contaminants from the surface, piranha cleaning also makes Au surface hydrophilic via allowing the adhesive force between water molecules and Au surface to dominate over cohesive force between water molecules. This hydrophilicity helps a strong analyte attachment on the surface by physisorption, and prevents leakage during the analyte incubation inside the sample preparation kit.

4.2. Analyte immobilization

Attachment of analytes on Au surface was realized via physisorption. First, 200 μg/mL protein A/G was incubated on the chip surface. Protein A/G binds on Au surface through physisorption. Following this, 100 μg/mL protein IgG was incubated on Au surface, which binds on protein A/G through its Fc region. After each protein incubation, chip surface was rinsed with PBS and DI-water to remove unbound protein from the surface. Patient-derived H1N1 viruses were received as a kind gift from the Department of Medical Microbiology, Ege University, Izmir, Turkey. Titer of the H1N1 virus was determined as 10^7 $TCID_{50}$/mL. Ten-fold serial dilutions of the H1N1 virus were prepared in sterile PBS. Then, the virus solution was incubated on the chip surface at room temperature followed by a wash step with sterile PBS. Virus immobilization step was performed in a Biosafety Level 2 (BSL-2) laboratory. Here, the incubation time for each analyte was chosen as 1 h, which could alter for different temperatures as it is an important parameter governing the protein binding kinetics.

4.3. Spectroscopy analysis

The plasmonic chip was illuminated with a broadband white LED light source. The light transmitted from the chip was collected by an objective lens and fiber-coupled to a spectrometer with 0.09 nm spectral resolution. The experimental data was smoothened with a Savitzky – Golay filter, [42] $Y_j = \sum_{i=\frac{1-m}{2}}^{\frac{m-1}{2}} C_i y_{j+1}, \frac{m-1}{2} \le j \le n - \frac{m-1}{2}$, where $n\{x_j, y_j\}$ is the number EOT data, y is the EOT data, x is the wavelength, and Y is the smoothened EOT data. EOT data was processed with m series of C convolution coefficients.

Author Contributions

A.E.C. conceived the idea. A.E.C. constructed the optical instruments and sample preparation kit, and fabricated the plasmonic samples. S.N.T. performed the physisorption based surface modification, and Z.A.K. performed virus immobilization. A.E.C. performed data acquisition and analyses. Z.A.Y. coded Python™ GUI. A.E.C., Z.A.K. and S.N.T. discussed the results and wrote the manuscript. All authors contributed to editing and preparing the manuscript.

CRediT authorship contribution statement

Arif E. Cetin: Conceptualization, Methodology, Software, Validation, Formal analysis, Data curation, Writing - original draft, Writing - review & editing, Supervision, Funding acquisition. **Zeynep A. Kocer:** Methodology, Writing - original draft, Writing - review & editing, Supervision. **Seda Nur Topkaya:** Methodology, Validation, Data curation, Writing - original draft, Writing - review & editing. **Ziya Ata Yazici:** Software, Validation.

Declaration of Competing Interest

The authors declare that they have no known competing financial interests or personal relationships that could have appeared to influence the work reported in this paper.

Acknowledgments

A.E.C. acknowledges The Scientific and Technological Research Council of Turkey (TUBITAK) 2232 – Career Integration Fellowship (Project No. 119C002), and BAGEP Award of the Science Academy, Turkey. Authors thank Buket Onder for the illustrations.

Appendix A. Supplementary data

Supplementary material related to this article can be found, in the online version, at doi:https://doi.org/10.1016/j.snb.2021.130301.

References

[1] A.A. Yanik, M. Huang, O. Kamohara, A. Artar, T.W. Geisbert, J.H. Connor, H. Altug, An optofluidic nanoplasmonic biosensor for direct detection of live viruses from biological media, Nano Lett. 10 (2010) 4962–4969, https://doi.org/10.1021/nl103025u.

[2] M.Z. Tay, C.M. Poh, L. Rénia, P.A. MacAry, L.F.P. Ng, The trinity of COVID-19: immunity, inflammation and intervention, Nat. Rev. Immunol. 20 (2020) 363–374, https://doi.org/10.1038/s41577-020-0311-8.

[3] J.D. Cherry, P. Krogstad, SARS: the first pandemic of the 21st century, Pediatr. Res. 56 (2004) 1–5, https://doi.org/10.1203/01.PDR.0000129184.87042.FC.
[4] G.J.D. Smith, D. Vijaykrishna, J. Bahl, S.J. Lycett, M. Worobey, O.G. Pybus, S. K. Ma, C.L. Cheung, J. Raghwani, S. Bhatt, J.S.M. Peiris, Y. Guan, A. Rambaut, Origins and evolutionary genomics of the 2009 swine-origin H1N1 influenza a epidemic, Nature. 459 (2009) 1122–1125, https://doi.org/10.1038/nature08182.
[5] C.S. Wood, M.R. Thomas, J. Budd, T.P. Mashamba-Thompson, K. Herbst, D. Pillay, R.W. Peeling, A.M. Johnson, R.A. McKendry, M.M. Stevens, Taking connected mobile-health diagnostics of infectious diseases to the field, Nature 566 (2019) 467–474, https://doi.org/10.1038/s41586-019-0956-2.
[6] K. Sedlak, Ruth Hall; jerome, viral diagnostics in the era of digital PCR, Diagn. Microbiol. Infect. Dis. 75 (2014) 1–4, https://doi.org/10.1016/j.diagmicrobio.2012.10.009.Viral.
[7] M. Niikura, T. Ikegami, M. Saijo, I. Kurane, M.E. Miranda, S. Morikawa, Detection of Ebola viral antigen by enzyme-linked immunosorbent assay using a novel monoclonal antibody to nucleoprotein, J. Clin. Microbiol. 39 (2001) 3267–3271, https://doi.org/10.1128/JCM.39.9.3267-3271.2001.
[8] A. Hematian, N. Sadeghifard, R. Mohebi, M. Taherikalani, A. Nasrolahi, M. Amraei, S. Ghafourian, Traditional and modern cell culture in virus diagnosis, osong public heal, Res. Perspect. 7 (2016) 77–82, https://doi.org/10.1016/j.phrp.2015.11.011.
[9] A. Ahmed, J.V. Rushworth, N.A. Hirst, P.A. Millner, Biosensors for whole-cell bacterial detection, Clin. Microbiol. Rev. 27 (2014) 631–646, https://doi.org/10.1128/CMR.00120-13.
[10] S. Sang, Y. Wang, Q. Feng, Y. Wei, J. Ji, W. Zhang, Progress of new label-free techniques for biosensors: a review, Crit. Rev. Biotechnol. 36 (2016) 465–481, https://doi.org/10.3109/07388551.2014.991270.
[11] M. Soler, C.S. Huertas, L.M. Lechuga, Label-free plasmonic biosensors for point-of-care diagnostics: a review, Expert Rev. Mol. Diagn. 19 (2019) 71–81, https://doi.org/10.1080/14737159.2019.1554435.
[12] X. Fan, I.M. White, S.I. Shopova, H. Zhu, J.D. Suter, Y. Sun, Sensitive optical biosensors for unlabeled targets: a review, Anal. Chim. Acta 620 (2008) 8–26, https://doi.org/10.1016/j.aca.2008.05.022.
[13] X. Luo, J.J. Davis, Electrical biosensors and the label free detection of protein disease biomarkers, Chem. Soc. Rev. 42 (2013) 5944–5962, https://doi.org/10.1039/c3cs60077g.
[14] E.B. Bahadir, M.K. Sezgintürk, A review on impedimetric biosensors, Artif. Cells, Nanomed. Biotechnol. 44 (2016) 248–262, https://doi.org/10.3109/21691401.2014.942456.
[15] S. Mehrabani, A.J. Maker, A.M. Armani, Hybrid integrated label-free chemical and biological sensors, Sens. (Switzerland). 14 (2014) 5890–5928, https://doi.org/10.3390/s140405890.
[16] C. Chen, J. Wang, Optical biosensors: an exhaustive and comprehensive review, Analyst 145 (2020) 1605–1628, https://doi.org/10.1039/c9an01998g.
[17] S.M. Borisov, O.S. Wolfbeis, Optical biosensors, Chem. Rev. 108 (2008) 423–461, https://doi.org/10.1021/cr068105t.
[18] M.A. Cooper, Optical biosensors in drug discovery, Nat. Rev. Drug Discov. 1 (2002) 515–528, https://doi.org/10.1038/nrd838.
[19] A. Belushkin, F. Yesilkoy, J.J. González-López, J.C. Ruiz-Rodríguez, R. Ferrer, A. Fàbrega, H. Altug, Rapid and digital detection of inflammatory biomarkers enabled by a novel portable nanoplasmonic imager, Small 16 (2020), https://doi.org/10.1002/smll.201906108.
[20] Y. Liu, Q. Liu, S. Chen, F. Cheng, H. Wang, W. Peng, Surface plasmon resonance biosensor based on smart phone platforms, Sci. Rep. 5 (2015) 1–9, https://doi.org/10.1038/srep12864.
[21] H. Šípová, M. Piliarik, M. Vala, K. Chadt, P. Adam, M. Bocková, K. Hegnerová, J. Homola, Portable surface plasmon resonance biosensor for detection of nucleic acids, Procedia Eng. 25 (2011) 148–151, https://doi.org/10.1016/j.proeng.2011.12.037.
[22] J.F. Masson, Portable and field-deployed surface plasmon resonance and plasmonic sensors, Analyst 145 (2020) 3776–3800, https://doi.org/10.1039/d0an00316f.
[23] T.Y. Chang, M. Huang, A.A. Yanik, H.Y. Tsai, P. Shi, S. Aksu, M.F. Yanik, H. Altug, Large-scale plasmonic microarrays for label-free high-throughput screening, Lab Chip 11 (2011) 3596–3602, https://doi.org/10.1039/c1lc20475k.
[24] A.E. Cetin, P. Iyidogan, Y. Hayashi, M. Wallen, K. Vijayan, E. Tu, M. Nguyen, A. Oliphant, Plasmonic sensor could enable label-free DNA sequencing, ACS Sens. 3 (2018), https://doi.org/10.1021/acssensors.7b00957.
[25] X. Li, M. Soler, C.I. Ozdemir, A. Belushkin, F. Yesilkoy, H. Altug, Plasmonic nanohole array biosensor for label-free and real-time analysis of live cell secretion, Lab Chip 17 (2017) 2208–2217, https://doi.org/10.1039/c7lc00277g.
[26] J.A. Jackman, E. Linardy, D. Yoo, J. Seo, W.B. Ng, D.J. Klemme, N.J. Wittenberg, S. H. Oh, N.J. Cho, Plasmonic nanohole sensor for capturing single virus-like particles toward virucidal drug evaluation, Small 12 (2016) 1159–1166, https://doi.org/10.1002/smll.201501914.
[27] M. Huang, B.C. Galarreta, A.E. Cetin, H. Altug, Actively transporting virus like analytes with optofluidics for rapid and ultrasensitive biodetection, Lab Chip 13 (2013) 4841–4847, https://doi.org/10.1039/c3lc50814e.
[28] A.G. Brolo, Plasmonics for future biosensors, Nat. Photonics 6 (2012) 709–713, https://doi.org/10.1038/nphoton.2012.266.
[29] A.E. Cetin, A.F. Coskun, B.C. Galarreta, M. Huang, D. Herman, A. Ozcan, H. Altug, Handheld high-throughput plasmonic biosensor using computational on-chip imaging, Light Sci. Appl. 3 (2014), https://doi.org/10.1038/lsa.2014.3.
[30] A.F. Coskun, A.E. Cetin, B.C. Galarreta, D.A. Alvarez, H. Altug, A. Ozcan, Lensfree optofluidic plasmonic sensor for real-time and label-free monitoring of molecular binding events over a wide field-of-view, Sci. Rep. 4 (2014) 1–7, https://doi.org/10.1038/srep06789.
[31] A.E. Cetin, D. Etezadi, B.C. Galarreta, M.P. Busson, Y. Eksioglu, H. Altug, Plasmonic nanohole arrays on a robust hybrid substrate for highly sensitive label-free biosensing, ACS Photonics 2 (2015) 1167–1174, https://doi.org/10.1021/acsphotonics.5b00242.
[32] A.E. Cetin, A. Mertiri, M. Huang, S. Erramilli, H. Altug, Thermal tuning of surface plasmon polaritons using liquid crystals, Adv. Opt. Mater. 1 (2013), https://doi.org/10.1002/adom.201300303.
[33] A.E. Cetin, S.N. Topkaya, O. Yalcin-Ozuysal, A. Khademhosseini, Refractive index sensing for measuring single cell growth, ACS Nano (2021), https://doi.org/10.1021/acsnano.1c04031.
[34] A.E. Cetin, S.N. Topkaya, Plasmonic diffraction field pattern imaging could resolve ultrasensitive bioinformation, ACS Photonics 6 (2019) 2626–2635, https://doi.org/10.1021/acsphotonics.9b01076.
[35] A.E. Cetin, S.N. Topkaya, Photonic crystal and plasmonic nanohole based label-free biodetection, Biosens. Bioelectron. 132 (2019) 196–202, https://doi.org/10.1016/j.bios.2019.02.047.
[36] A.A. Yanik, A.E. Cetin, M. Huang, A. Artar, S.H. Mousavi, A. Khanikaev, J. H. Connor, G. Shvets, H. Altug, Seeing protein monolayers with naked eye through plasmonic Fano resonances, Proc. Natl. Acad. Sci. 108 (2011) 11784–11789, https://doi.org/10.1073/pnas.1101910108.
[37] Y. Li, Y. Yuan, X. Peng, J. Song, J. Liu, J. Qu, An ultrasensitive Fano resonance biosensor using two dimensional hexagonal boron nitride nanosheets: theoretical analysis, RSC Adv. 9 (2019) 29805–29812, https://doi.org/10.1039/c9ra05125b.
[38] K.L. Lee, J. Bin Huang, J.W. Chang, S.H. Wu, P.K. Wei, Ultrasensitive biosensors using enhanced fano resonances in capped gold nanoslit arrays, Sci. Rep. 5 (2015) 1–9, https://doi.org/10.1038/srep08547.
[39] I. Fernandez-Cuesta, M.M. West, E. Montinaro, A. Schwartzberg, S. Cabrini, A nanochannel through a plasmonic antenna gap: an integrated device for single particle counting, Lab Chip 19 (2019) 2394–2403, https://doi.org/10.1039/c9lc00186g.
[40] A. Portela, O. Calvo-Lozano, M. Estevez, A. Medina Escuela, L.M. Lechuga, Optical nanogap antennas as plasmonic biosensors for the detection of miRNA biomarkers, J. Mater. Chem. B. 8 (2020) 4310–4317, https://doi.org/10.1039/d0tb00307g.
[41] M. Soler, A. Belushkin, A. Cavallini, C. Kebbi-Beghdadi, G. Greub, H. Altug, Multiplexed nanoplasmonic biosensor for one-step simultaneous detection of Chlamydia trachomatis and Neisseria gonorrhoeae in urine, Biosens. Bioelectron. 94 (2017) 560–567, https://doi.org/10.1016/j.bios.2017.03.047.
[42] W.H. Press, S.A. Teukolsky, Savitzky-golay smoothing filters, Comput. Phys. 4 (1990) 669, https://doi.org/10.1063/1.4822961.

Arif E. Cetin is a Research Group Leader in Izmir Biomedicine and Genome Center in Izmir, Turkey. He received his Ph.D. degree in 2013 at the Department of Electrical Engineering, Boston University, Boston, MA, USA. He worked as a post-doctoral associate at EPFL, Switzerland and MIT, Massachusetts, MA, USA and research scientist at Omniome, Inc. San Diego, CA, USA. Dr. Cetin pursues research on optical nano-biosensors integrated with microfluidics, handheld biosensors for high-throughput and multiplexed biosensing, electromechanical sensors for growth rate cytometry, and label-free techniques for DNA sequencing.

Seda Nur Topkaya completed her Ph.D in 2013 at Analytical Chemistry, Faculty of Pharmacy, Ege University Ege University, Izmir, Turkey. She is an Associate Professor at Analytical Chemistry and the head of both Basic Pharmaceutical Sciences and the Department of Analytical Chemistry at Izmir Katip Celebi University. Her main research interests are electrochemistry, biosensors, drug-biomolecule interactions, electrochemical-based DNA biosensors and tissue engineering applications. She has published more than 30 papers in SCI indexed journals and serving as reviewer-editorial board member of numerous international journals.

Zeynep Ahsen Kocer completed her PhD in 2010 at the Department of Biological Sciences, Bowling Green State University in OH, USA. She pursued postdoctoral research at the Virology Division of the Department of Infectious Diseases at St. Jude Children's Research Hospital in Memphis, TN, USA. She worked as a Staff Scientist at the Influenza Research Institute at the University of Wisconsin-Madison. Dr. Kocer is currently working as a Research Group Leader at the Emerging Viral Diseases Laboratory at Izmir Biomedicine and Genome Center. Her research interests mainly focus on the emergence of novel zoonotic viruses and their risk assessment in terms of pandemic potential. She is also holding an Assistant Professor position at the Department of Biomedicine and Health Technologies at Izmir International Biomedicine and Genome Institute, Dokuz Eylul University.

Ziya Ata Yazici is an undergraduate student at the Department of Biomedical Engineering, TOBB University of Economics and Technology, Ankara, Turkey. His research interests mainly focus on image processing, deep learning and machine learning techniques.